J Mater Sci (2017) 52:8455–8464

Polymers

Cellulose nanofiber/cationic conjugated polymer hybrid aerogel sensor for nitroaromatic vapors detection

Jingjing Qin[1,2], Lang Chen[1,*], Chenghui Zhao[2], Qixiang Lin[3], and Shaowei Chen[4]

[1] School of Mechatronical Engineering, Beijing Institute of Technology, Beijing 100081, China
[2] Fuzhou Command Academy of Armed Police Force, Fuzhou, China
[3] Armed Police Force Engineering University, Xi'an, China
[4] Fujian Division of the Chinese People's Armed Police Force, Fujian, China

Received: 8 February 2017
Accepted: 28 March 2017
Published online: 7 April 2017

ABSTRACT

A novel porous aerogel of cellulose nanofiber (CNF)/cationic water-soluble poly[9,9-bis[3′-(*N*,*N*-dimethy)-*N*-ethylammonium)propyl)-2,7-fluorene-*alt*-1,4-phenylene]dibromide (CPFD) is prepared by freeze drying. CNF can effectively prevent aggregation of the conjugated polymer CPFD backbones. The CNF/CPFD hybrid aerogel is use for the detection of nitroaromatic (NAC) vapors. Due to the porous structure, the CNF/CPFD hybrid aerogel possesses a large number of accessible cavities, which could be sufficiently large to allow the diffusion of NAC vapors into the aerogel. As a result, the CNF/CPFD aerogel sensor shows high sensitivity toward NAC vapors. For 120-s exposure, the fluorescence quenching efficiency of the CNF/CPFD aerogel sensor toward 2,4-dinitrotoluene vapor is up to 85.9%, which is much larger than that of the spin-cast CPFD film. Furthermore, the sensing performance of the CNF/CPFD hybrid aerogel is not heavily dependent on the thickness, and the sensing process of the CNF/CPFD aerogel sensor is reversible.

Introduction

One increasing concern in environmental safety control and homeland security is the simple and sensitive trace detection of explosives vapors [1–3]. Most explosives are nitro-substituted compounds. Typically, NAC explosives, such as 2,4,6-trinitrotoluene (TNT), DNT and picric acid (PA), are the principle components of military explosives and landmines [4, 5]. Usually, trace detection is limited to the more volatile explosives, such as DNT and TNT, whose equilibrium vapor pressures are about 100 and 5 ppb, respectively [6]. Although many explosive-detection instruments are widely utilized [7, 8], these devices are generally expensive and require professional operation, which are not applicable for on-site field testing. Alternatively, fluorescence sensors based on conjugated polymer (CP) have been regarded as an excellent candidate for the rapid detection of NACs [9]. Indeed, the electron-withdrawing effect of the nitro groups makes the NAC highly electron-deficient and easily

Address correspondence to E-mail: chenlang_bit@126.com

DOI 10.1007/s10853-017-1065-y

to accept electrons from excited CPs. The fluorescence quenching is caused by association of electron-deficient NAC with electron-rich CP via electron-transfer mechanism [10].

CP-based detection has many advantages over traditional detection methods in virtue of the high sensitivity, simplified operation, and superquenching effects toward NAC [11, 12]. Therefore, solid-state CP films using spin-casting technique are generally desired for NAC vapor detection. However, the spin-cast CP film thickness seriously affects the sensing performance of these film sensors, mainly because the rigid CP film prevents the diffusion of analyte vapors [13]. In addition, the aggregation behavior of CP backbones in a solid film state would result in serious self-quenching of fluorescent intensities [14]. In order to minimize the reliance of sensing performance on film thickness and to hinder aggregation of the CP backbones, a highly porous hybrid aerogel could be a solution, mainly because of its large surface area, effective porosity, and easy permeability of fluorescent sensors.

Cellulose nanofiber (CNF) prepared from cellulose has some superior performances, such as excellent machinability, inexpensive, environmentally friendly [15]. Furthermore, CNF was prepared by selectively introducing large amounts of C-6 carboxyl groups on each cellulose microfibril surface [16]. Importantly, the CNF suspension has good aerogel-forming property [17]. CNF-based aerogels display a highly porous structure and porosity [18]. Therefore, compared with other species, such as silica nanoparticles [19], cellulose [20], glass [21], it might be a wise choice to use CNF as an ideal substrate of CP-based fluorescent sensors for potential application.

In this paper, we report a novel porous CNF/CPFD hybrid aerogel as a sensor for the detection of NAC vapors. The cationic CPFD is selected as the fluorophore, because it has good water solubility and can form electrostatic interaction with C-6 carboxyl groups of CNF in water. In addition, CNF can effectively prevent aggregation of CPFD backbones. The highly porous structure of the CNF/CPFD aerogel prepared by freeze drying can generate accessible cavities, which can benefit the rapid diffusion of NAC vapors into the hybrid aerogel. As expected, the CNF/CPFD hybrid aerogel shows high sensitivity toward NAC vapors.

Materials and methods

Materials

2,7-Dibromo-9,9-bis[3,3′-(*N*,*N*-dimethylamino)propyl] fluorine was purchased from Tokyo Chemical Industry Co., Ltd. Benzen-1,4-bis(boronic acid)-propane-1,3-dioldiester was obtained from Synwit Technology Co., Ltd. 2,2,6,6-tetramethylpiperidine-1-oxyl (TEMPO, 98 wt%) and tetrakis(triphenylphosphine) palladium ($Pd(PPh_3)_4$) were purchased from Aladdin-Reagent Co., Ltd. Never-dried hardwood bleached kraft pulp fibers, other reagents, and solvents obtained from commercial suppliers were used without further purification.

Characterization

UV spectra were recorded on a Shimadzu UV-1700 Ultraviolet spectrophotometer. Fluorescence spectra were recorded by Hitachi F-4500 Fluorescence spectrophotometer. Rheological tests were conducted on a Physica MCR 301 Rheometer with 25-mm-diameter parallel-plate geometry at 25 °C. Gel permeation chromatography (GPC) was operated by a Waters GPC515-2410 System with THF as an eluant. X-ray photoelectron spectroscopy (XPS) was measured on an AXIS Ultra DLD spectrometer using Al Kα radiation. Scanning electron microscopy (SEM) images were taken using a Hitachi S-4800 field-emission-gun scanning electron microscope operated at 15 kV. Nitrogen sorption measurements were performed with a BELSORP-Mini II (MicrotracBEL, Japan) to obtain pore properties such as the BET-specific surface area. Zeta potential was measured by using a Zetasizer Nano ZS90 (Malvern Instrument, UK). Fluorescence quantum efficiencies (Φ_F) in solution and solid state were determined relative to equiabsorbing solutions of anthracene ($\Phi_F = 0.27$ in hexane) and film of $\sim 10^{-3}$ M 9,10-diphenylanthracene in poly(methyl methacrylate) (PMMA) ($\Phi_F = 0.83$), respectively [13].

Synthesis of cationic, water-soluble conjugated polymer (CPFD)

Cationic CPFD was prepared by following previous literature with a slight modification [22]: 2,7-dibromo-9,9-bis[3,3′-(*N*,*N*-dimethylamino)propyl]fluorine (494 mg), and benzene-1,4-bis(boronic acid)propane-1,3-dioldiester (246 mg) were dissolved in THF

(15 mL). K_2CO_3 aqueous solution (2 mol/L, 10 mL) was then added, and the mixture was stirred under a nitrogen atmosphere for 30 min. After adding the catalyst of $Pd(PPh_3)_4$ (24 mg), the mixture was stirred at reflux (about 69 °C) for 48 h under nitrogen. After being cooled to room temperature, the mixture was removed into methanol (60 mL). The precipitates were collected by filtration and rinsed repeatedly with methanol and water. Then, the precipitates were Soxhlet extracted with acetone for 40 h. Finally, the polymer PFD was dried under vacuum at 40 °C for 2 days.

The resulting PFD (100 mg) was dissolved in THF/DMSO (50 mL, 4:1, v/v), to which was added bromoethane (2 g, 18 mmol). The mixture was heated at 50 °C for 5 days. Once precipitates were observed, some water was added to dissolve them. After the reaction was finished, THF, water, and extra bromoethane were evaporated in vacuum, and the DMSO phase was poured into diethyl ether (100 mL). The precipitate was collected by centrifugation and washed with acetone. Finally, the CPFD ($\bar{M}_n$: 6980, PDI: 1.68) was dried under vacuum at 40 °C for 2 days.

Preparation of cellulose nanofiber (CNF) dispersion

CNF dispersion was synthesized by following a previously reported procedure [23]: TEMPO (0.016 g) and sodium bromide (0.16 g) were dissolved in water (100 mL). Then, cellulose fibers (1 g) were added to this solution. The NaClO solution (15 mmol/g cellulose) was added to the mixture. Under fixed pH value of 10, the solution reacted at 25 °C for 4 h. Then, the oxidized cellulose was collected by filtration and washed repeated with distilled water. After 6-min sonication under 300 W power, CNF dispersion was centrifuged at 10000*g* for 15 min.

Preparation of the CNF/CPFD aerogel

CPFD (50 mg) was dissolved in distilled water (10 mL), and CNF dispersion (20 g, 0.25 wt%) was added to this solution. With 15 min sonicating time under 300 W power, the mixture CNF/CPFD suspension became homogeneous. The CNF/CPFD suspension was poured into mold with a thickness of 1 mm. Afterward, it was exposed to the hydrochloric acid vapor for about 12 h to form CNF/CPFD hydrogel at about 4 °C. Then, the CNF/CPFD hydrogel was washed with distilled water several times until it was neutral. The recovery ratio of CPFD in the CNF/CPFD hydrogel against the amount of CPFD we added is 38%. Finally, the resulting hydrogel was quickly immersed in liquid nitrogen for 0.5 h, followed by lyophilization in a freeze drier (SCIENTZ-10 N, NingBo Scientz Co., Ltd., China) for 20 h to obtain the CNF/CPFD hybrid aerogel.

Synthesis of the spin-cast CPFD film

The CPFD (8 mg) was dissolved in THF (20 mL). Then, this solution was spin-casted onto a quartz substrate (microscope slide, length 15 mm, and width 15 mm) at a spin rate of 3000 rpm. Finally, the CPFD film was obtained after leaving it under vacuum at 30 °C for 2 days.

Fluorescence quenching experiment

The fluorescence sensing performance of the CNF/CPFD hybrid aerogel was investigated toward NAC vapors in the following manner [24]. Briefly, the CNF/CPFD hybrid aerogel was inserted into a glass vial (25 mL volume) containing solid analytes and cotton gauze at room temperature. Cotton gauze could prevent direct contact between the aerogel and analytes and benefit to maintain a constant saturated vapor pressure. After the CNF/CPFD hybrid aerogel was inserted into the glass vial with the analyte vapor for a certain period time, the fluorescence spectrum of the hybrid aerogel was recorded immediately at excitation wavelength of 386 nm. All measurements were taken in ambient atmosphere. The following equation (Eq. 1) was used to characterize the fluorescence quenching efficiency [25]:

$$\eta = (I_0 - I)/I_0 \quad (1)$$

where η is the fluorescence quenching efficiency, I_0 is the fluorescence intensity without the quencher vapor, and I is the fluorescence intensity after adding quencher vapor.

Results and discussion

Synthesis and characterization

Scheme 1 shows the synthesis of the cationic conjugated polymer CPFD. The CPFD exhibits good water

Scheme 1 The synthesis of the cationic CPFD.

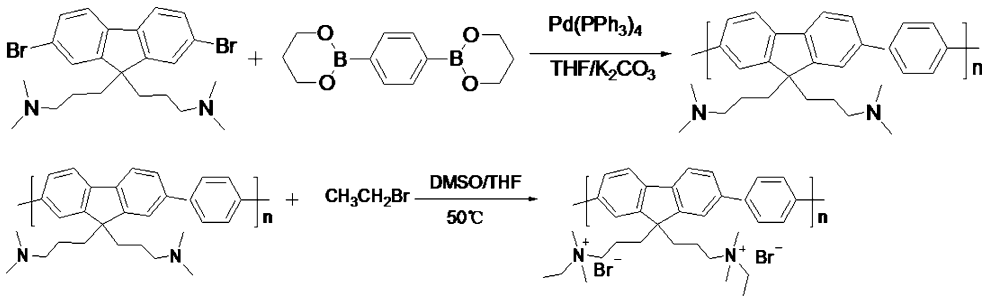

Scheme 2 The formation of the CNF/CPFD hybrid aerogel and the detecting principle for DNT vapor.

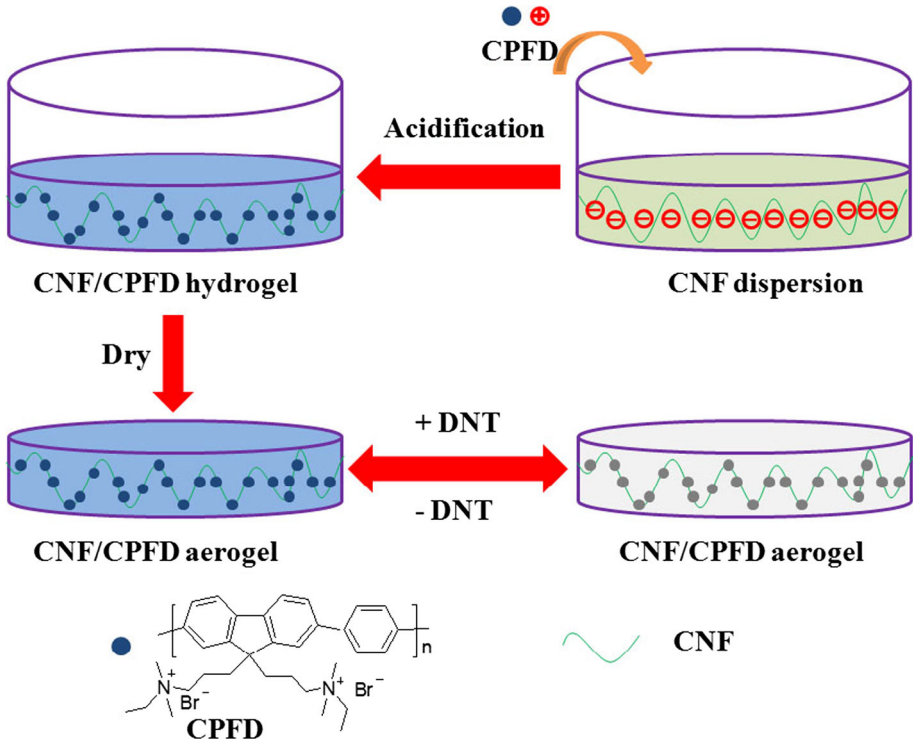

solubility. The formation process of the CNF/CPFD hybrid aerogel and the detecting principle for DNT vapor are shown schematically in Scheme 2. With the help of sonication, CPFD could be well dispersed in the CNF dispersion to form a stable CNF/CPFD suspension, which can maintain stability for several months at room temperature. Therefore, CNF can be used as an environmentally friendly dispersant of water-soluble CPFD.

With the aid of hydrochloric acid vapor, the CNF/CPFD hydrogel could be obtained from the CNF/CPFD suspension. The CNF/CPFD hydrogel and CNF hydrogel are characterized by rheology measurements, which are shown in Fig. 1a. For the CNF/CPFD hydrogel and CNF hydrogel, the storage modulus (G′) values are all an order of magnitude higher than the loss modulus (G″) values. This phenomenon indicates that the CNF/CPFD hydrogel and CNF hydrogel are of a permanent network. In addition, the storage modulus (G′) value of the CNF/CPFD hydrogel is much higher than that of pure CNF hydrogel. This indicates that the permanent network of CNF is obviously changed by cationic CPFD. Furthermore, the mechanical strength of CNF/CPFD hydrogel is much higher than that of the CNF hydrogel. Since CNF hydrogel is obtained by hydrogen bonds [26], these results implied that there is another strong interaction between CNF and CPFD. The zeta potential value of the CNF dispersion (0.17 wt%) is about −73.4 mV, which means that large amounts of carboxyl groups were on the CNF surface. In addition, the zeta potential value of CPFD solution in water (1.67 mg/mL) is about +63.5 mV, indicating that CPFD is a cationic polymer. Therefore,

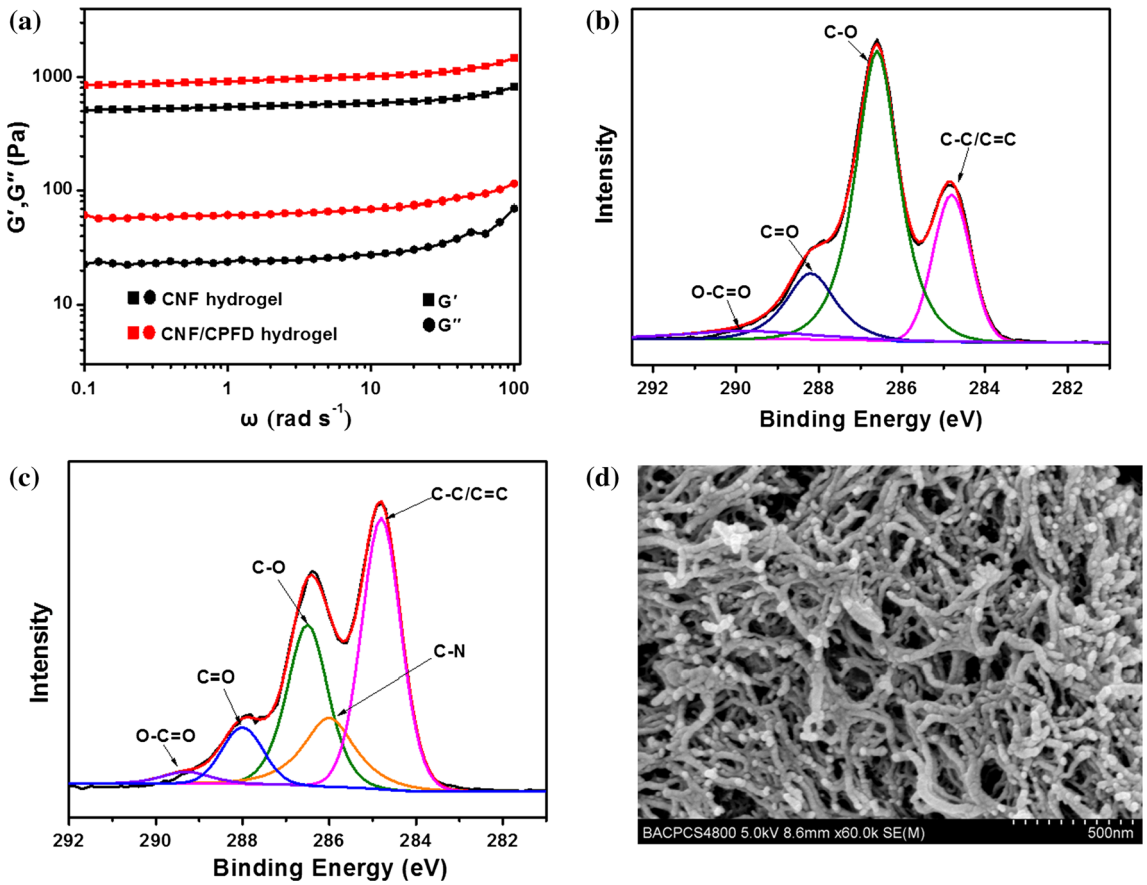

Figure 1 **a** Dynamic rheological behavior of the CNF hydrogel and CNF/CPFD hydrogel. C 1*s* XPS spectra for **b** CNF aerogel and **c** CNF/CPFD aerogel. **d** SEM image of the CNF/CPFD aerogel.

electrostatic interaction can be formed between CPFD and CNF.

The CNF/CPFD hybrid aerogel is prepared by the CNF/CPFD hydrogel via freeze drying. X-ray photoelectron spectroscopy (XPS) is used for characterizing the surface chemistry of the CNF/CPFD hybrid aerogel. Figure 1b, c shows C 1*s* spectra of the CNF aerogel and CNF/CPFD hybrid aerogel, respectively. The curves are fitted considering the following contributions: C=C/C–C (284.4 eV), C–N (286.0 eV), C–O (286.6 eV), C=O (288.4 eV), O–C=O (289.8 eV). Compared with CNF aerogel, the C=C/C–C peak intensity of the CNF/CPFD aerogel increases obviously. In addition, the new peak of C–N appears for the CNF/CPFD aerogel. These results indicate that CPFD has been well preserved in the CNF/CPFD aerogel.

The morphology of the CNF/CPFD hybrid aerogel is characterized by SEM image, which is shown in Fig. 1d. The porous morphology of the CNF/CPFD hybrid aerogel is quite uniform on the large scale. This indicates that the uniformly dispersed states of CPFD are effectively preserved in the CNF/CPFD hybrid aerogel. In addition, the CNF/CPFD hybrid aerogel possesses a three-dimensional highly porous structure. Nitrogen adsorption–desorption experiment further provides the pore characteristics of the CNF/CPFD hybrid aerogel. Figure 2a, b exhibits the N_2 isotherms and the Barrett–Joyner–Halenda (BJH) pore diameter distribution of the CNF/CPFD aerogel. The CNF/CPFD hybrid aerogel exhibits a type III isotherm. In addition, the Brunauer–Emmett–Teller (BET) specific surface area of the CNF/CPFD hybrid aerogel is about 1.41 $m^2\ g^{-1}$. From the pore size distribution calculated by the BJH method, much of the pore diameter lies in the 1.3–50 nm range. These results imply that the pore structures of the CNF/CPFD hybrid aerogel are dominated by mesopores, which could effectively increase the surface area and provide a large number of loose cavities. Therefore, it is probably a good decision to select the CNF/CPFD hybrid aerogel as a chemosensor for NAC vapors.

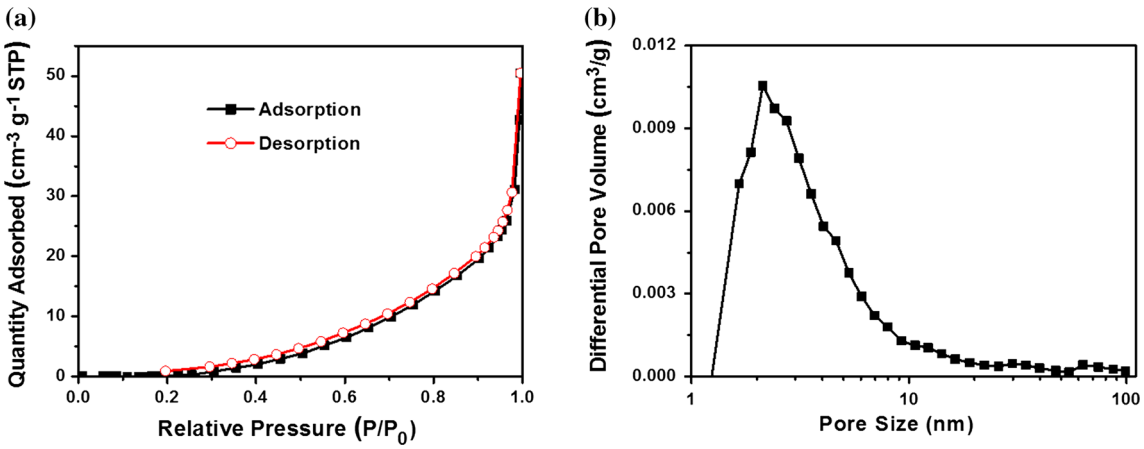

Figure 2 **a** N_2 adsorption and desorption isotherms and **b** BJH pore diameter distribution of the CNF/CPFD aerogel.

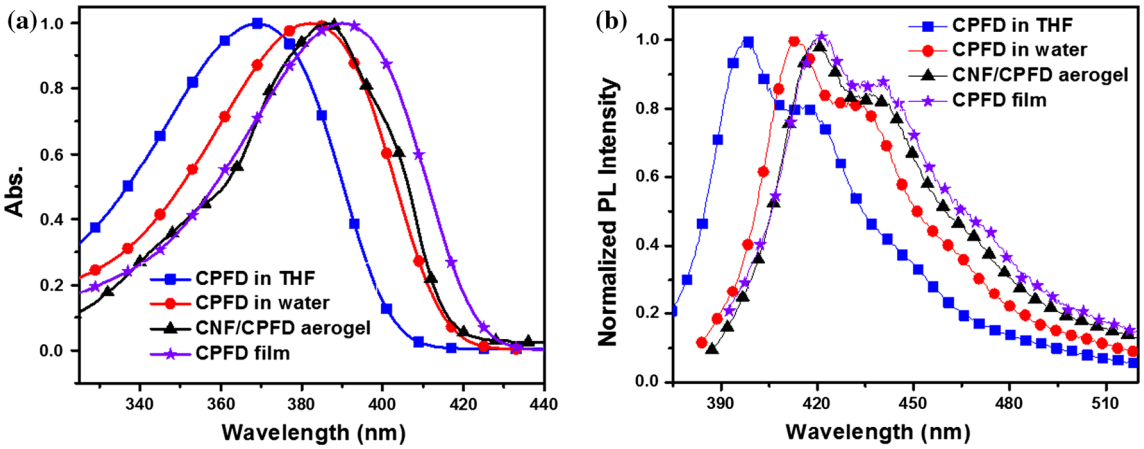

Figure 3 **a** The absorption and **b** fluorescence spectra of the CPFDs in two different solvents (water and THF, respectively), CNF/CPFD hybrid aerogel and CPFD film.

Photophysical properties

The UV–visible absorption and fluorescence spectra of the CPFD in two different solvents (water and THF, respectively), CNF/CPFD hybrid aerogel, and CPFD film are shown in Fig. 3a, b, respectively. The absorption maxima of CPFD in THF and water are observed at 369 and 382 nm, respectively. The corresponding fluorescence spectra are peaked at 398 and 414 nm with the vibronic shoulder located at 416 and 431 nm, respectively. Obviously, with the increase of solvent polarity, the absorption and fluorescence spectra of CPFD exhibit red shifts. In addition, the fluorescence quantum efficiency of CPFD in THF is 39.6%, which is higher than that of CPFD in water ($\Phi_F = 26.3\%$).That is because the chain aggregation of the CPFD main chain is increased in the polar solvent.

On the other hand, the absorption and fluorescence maxima for the spin-cast CPFD film are 390 and 424 nm, respectively, but those for the CNF/CPFD hybrid aerogel are 386 and 419 nm, respectively. Clearly, in contrast to the CNF/CPFD hybrid aerogel, the CPFD film displays a substantial red shift relative to solution values. It is also interesting to note that the fluorescence quantum efficiency of the CNF/CPFD aerogel is 15.5%, which is higher than that of the CPFD film ($\Phi_F = 8.4\%$). It is known that aggregation of conjugated polymers has generally been responsible for decreased fluorescence efficiencies [13, 27]. Therefore, the CNF/CPFD aerogel should have the ability to prevent aggregation of CPFD backbones,

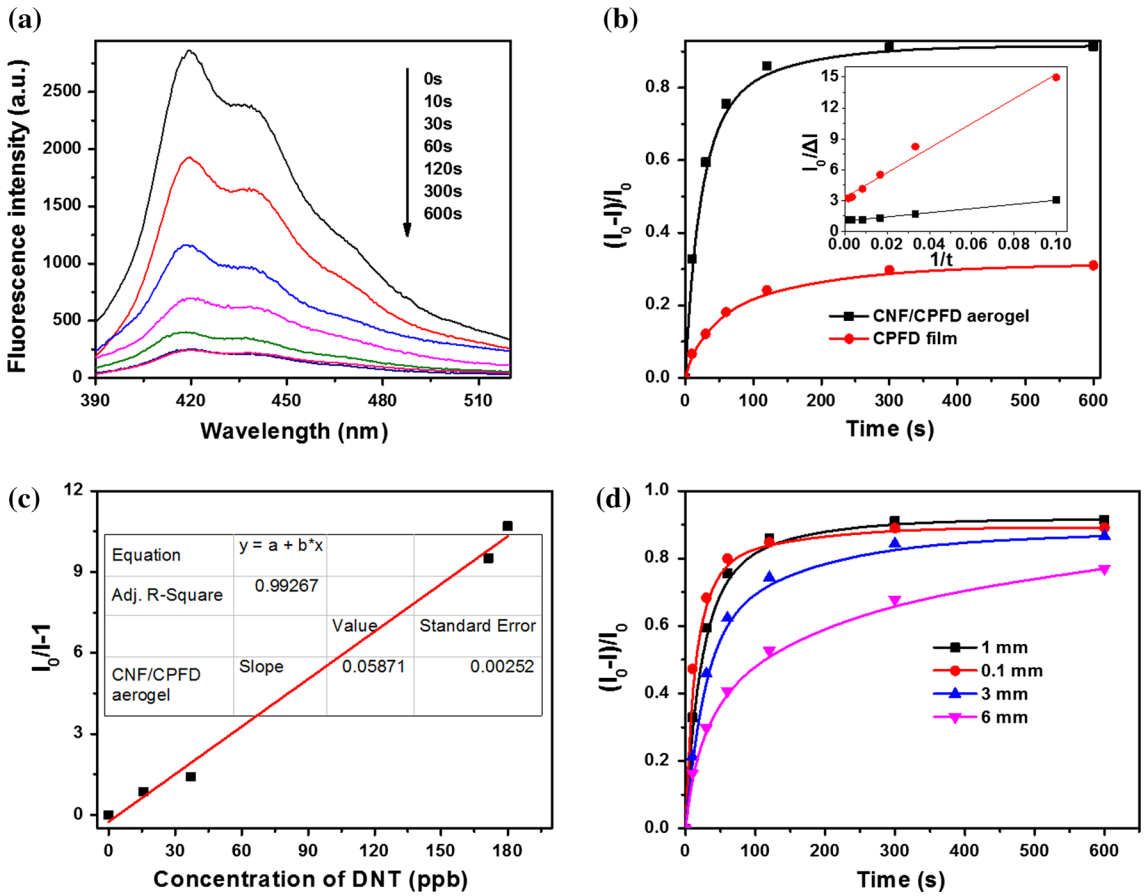

Figure 4 **a** Time-dependent fluorescence intensities of the CNF/CPFD aerogel upon exposure to DNT vapor. **b** Fluorescence quenching efficiencies of the CNF/CPFD hybrid aerogel and CPFD film upon exposure to DNT vapor at different times, respectively. *Inset* modified Stern–Volmer for the CNF/CPFD aerogel. **c** The Stern–Volmer plots as a function of DNT vapor concentration for the CNF/CPFD aerogel. **d** The effect of aerogel thickness on time-dependent fluorescence quenching efficiencies of the CNF/CPFD aerogel upon exposure to DNT vapor.

because CPFD can be loosely dispersed in the CNF/CPFD aerogel via electrostatic interaction.

Fluorescence quenching studies with DNT vapor

A representative set of the changes in the fluorescence spectra of the CNF/CPFD hybrid aerogel upon saturated DNT vapor are shown in Fig. 4a. The fluorescence intensity of the CNF/CPFD aerogel is quenched obviously as the exposure time prolonged. For a comparison, measurements of the fluorescence quenching of the CPFD film by DNT vapor are also taken. The fluorescence quenching efficiencies of the CNF/CPFD hybrid aerogel and CPFD film upon exposure to DNT vapor are shown in Fig. 4b. The fluorescence quenching efficiency of the CPFB film is only 24.1% for 120-s exposure, due to the dense structure of the spin-cast CPFD film hindering the penetration and diffusion of DNT vapor [12]. However, the fluorescence quenching efficiency of the CNF/CPFD hybrid aerogel is up to 85.9% for 120-s exposure, leading to a fast response toward DNT vapor. The reason is that the CNF/CPFD aerogel possesses a three-dimensional highly porous structure, which could effectively increase the large surface area and provide a large number of loose cavities benefiting the penetration and diffusion of DNT molecules.

The loose cavities were further analyzed using the modified Stern–Volmer equation [10]:

$$\frac{I_0}{\Delta I} = \frac{1}{f_a} + \frac{1}{f_a K_{SV}^a t} \quad (2)$$

In Eq. (2), I_0 is the fluorescence intensity without the quencher vapor, $\triangle I = I_0 - I$ is the fluorescence

intensity drop with the quencher vapor, f_a is the fraction of easily accessible cavities, t is the exposure time, and is the Stern–Volmer constant for quenching inside these cavities. The modified Stern–Volmer plots for the CNF/CPFD hybrid aerogel and CPFD film are shown as an inset to Fig. 4b. The f_a of the CPFD film is only 0.30. However, the f_a of the CNF/CPFD hybrid aerogel is up to be 0.98. The much more numbers of easily accessible cavities exist in the CNF/CPFD aerogel. Therefore, DNT vapor is easy to penetrate into the internal layer of the aerogel sensor, leading to rapid response sensitivity.

Moreover, quantitative evaluation of the detection limit of the CNF/CPFD aerogel toward DNT was performed, where different temperatures provide various levels of vapor pressures for DNT. The vapor pressures of DNT at 4, 10, 20 and 25 °C are 15.8, 37.0, 171.4 and 180 ppb, respectively [28, 29]. The quenching process can be analyzed by Stern–Volmer relationship:

$$I_0/I = 1 + K_{SV}[Q] \quad (3)$$

where K_{SV} is the Stern–Volmer quenching constant, and $[Q]$ is the concentration of DNT vapor [30]. By fitting the linear curves (Fig. 4c), the K_{SV} of the CNF/CPFD hybrid aerogel is 5.87×10^{-2} ppb^{-1}. The detection limit of the CNF/CPFD hybrid aerogel toward DNT vapor can be obtained from the equation of $C_L = 3S/K_{SV}$, where C_L is the value of the detection limit, and S is the standard deviation of the fluorescence intensity for the blank samples which has been measured 15 times [30]. The detection limit of the CNF/CPFD hybrid aerogel toward DNT vapor is 4.9 ppb, which is lower than the equilibrium vapor pressure of the trace detection for DNT vapor (about 100 ppb). Such low limit of detection is of great benefit to environmental safety control and homeland security.

In addition, the effect of aerogel thickness on time-dependent fluorescence quenching efficiency was investigated (Fig. 4d). With the increase of aerogel thickness, the quenching speed to reach a plateau is slightly decreased. For exposure time of 600 s, the highest quenching efficiency (91.4%) toward DNT vapor is obtained on a 1-mm-thick aerogel, compared to 89.1 and 86.6% on 0.1 and 3-mm-thick aerogel, respectively, indicating that the sensing performance of the CNF/CPFD aerogel is not heavily dependent on the thickness.

Interference from other chemicals

The fluorescence sensing properties of the CNF/CPFD hybrid aerogels toward TNT, PA, nitrobenzene (NB) and 2,4-dinitrophenylhydrazine (DNPH) are also performed. Figure 5a exhibits the quenching efficiency of the CNF/CPFD aerogel upon exposure to DNT, TNT, PA, NB and DNPH vapors, respectively. The fluorescence intensities of the CNF/CPFD aerogel are all gradually quenched over time after exposure to the above NAC vapors. However, these five NAC vapors exhibit different quenching behaviors for the CNF/CPFD aerogel. For 120-s exposure to TNT, the quenching efficiency is 78.9%. As for NB, 120-s exposure of the CNF/CPFD aerogel leads to 69.9% reduction. Nevertheless, 120-s exposure to DNT results in a quenching efficiency exceeding 85.9%. Clearly, the fluorescence of the CNF/CPFD aerogel exposed to DNT vapor is much more sensitive than to TNT and other NACs. However, the

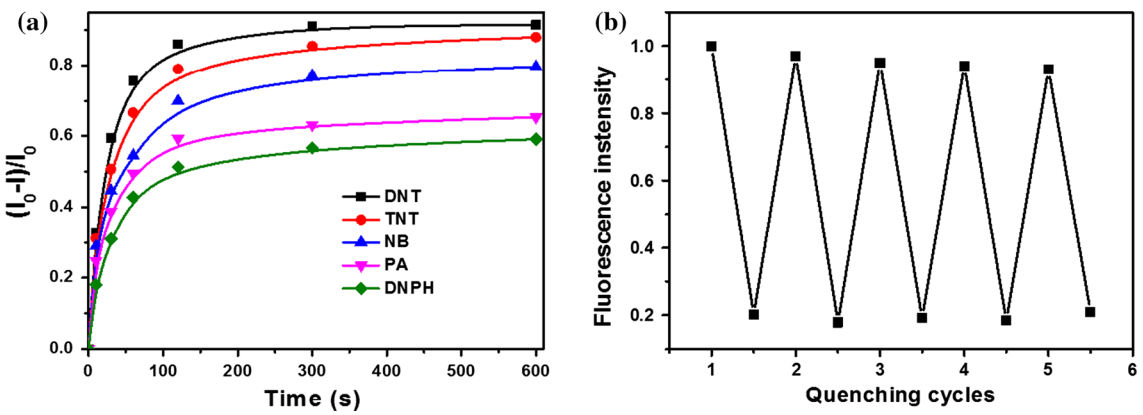

Figure 5 **a** Fluorescence quenching efficiencies of the CNF/CPFD aerogels upon exposure to DNT, TNT, PA, NB and DNPH vapors at different times, respectively. **b** The fluorescence quenching–recovery cycles test after the CNF/CPFD aerogel exposing to DNT for 60 s.

responses of the CNF/CPFD aerogel to PA and DNPH are much slower than to other NACs. For exposure time of 120 s, the fluorescence intensities of the CNF/CPFD aerogels are quenched 59.4 and 51.3%, respectively. Therefore, the quenching follows the order of DNT > TNT > NB > PA > DNPH.

Indeed, the dramatic difference can be attributed to their different vapor pressures. The vapor pressures of DNT, TNT, PA and DNPH are 1.74×10^{-4}, 8.02×10^{-6}, 5.80×10^{-9} and 1.26×10^{-9} mmHg at room temperature, respectively [31]. Generally speaking, for the quenching behavior of fluorescent CPs toward NAC vapors, with the increase of vapor pressure, the surface concentration of the CNF/CPFD aerogels is increased, which could produce remarkably fluorescence quenching. Thus, the considerable faster and greater quenching effect of DNT can be attributed to its high vapor pressure, while the poor performance of TNT, PA and DNPH is due to their low vapor pressure. However, although NB possesses higher vapor pressure (2.7×10^{-1} mmHg) [25], it shows lower quenching efficiency compared to other NAC. Besides vapor pressure, it has been reported that the exergonicity of electron transfer can also affect the quenching performance of NACs [13]. Because of the lower number of nitro groups (NO_2), the LUMO level of NB is higher than that of TNT and DNT, leading to higher reduction potential and lower electron accepting ability [32]. Thus, orbital energy matching of the LUMO levels of the CNF/CPFD aerogel and NB is not as good as that of the CNF/CPFD aerogel and TNT or DNT [33]. Therefore, NB has lower quenching efficiency.

Reversibility of the quenching process

The reversibility of the CNF/CPFD aerogel sensor is examined with DNT as an example nitroaromatic. The quenched CNF/CPFD aerogel by DNT vapor for 60 s was cleaned with methanol solvent several times. After drying in air, the fluorescence intensity of the CNF/CPFD aerogel sensor can be almost entirely recovered. When re-exposed to DNT for 60 s, the fluorescence of the CNF/CPFD aerogel sensor exhibits similar quench. After four times of quenching–regeneration cycles, the fluorescence intensity of the hybrid aerogel exhibits less than 6% loss. The results of the whole process are shown in Fig. 5b. Clearly, the sensing process of the CNF/CPFD aerogel is of good reversibility.

Conclusions

In conclusion, we have successfully designed and prepared the stable CNF/CPFD suspension by cross-linking sites with the assistance of ultrasonication. The CNF/CPFD hybrid aerogel is prepared from the CNF/CPFD hydrogel via freeze drying. CNF can provide large amount of C-6 carboxyl groups and effectively prevent aggregation of CPFD backbones. The CNF/CPFD hybrid aerogel is used as highly sensitive sensor for the detection of NAC vapors. Owing to a large number of loose cavities, the CNF/CPFD aerogel shows rapid response toward NAC vapors. The fluorescence quenching efficiency of the CNF/CPFD aerogel sensor is up to 85.9% for 120-s exposure to DNT vapor. In addition, the sensing performance of the CNF/CPFD aerogel is not heavily dependent on the thickness, and the novel hybrid aerogel shows good reversibility.

Compliance with ethical standards

Conflict of interest The authors declare that they have no conflict of interest.

References

[1] An N, Gonzalez CM, Sinelnikov R, Newman W, Sun S, Lockwood R, Veinot JGC, Meldrum A (2016) Detection of nitroaromatics in the solid, solution, and vapor phases using silicon quantum dot sensors. Nanotechnology. doi:10.1088/0957-4484/27/10/105501

[2] Zarei AR, Ghazanchayi B (2016) Design and fabrication of optical chemical sensor for detection of nitroaromatic explosives based on fluorescence quenching of phenol red immobilized polyvinyl alcohol) membrane. Talanta 150:162–168

[3] Kandpal M, Bandela AK, Hinge VK, Rao VR, Rao CP (2013) Fluorescence and piezoresistive cantilever sensing of trinitrotoluene by an upper-rim tetrabenzimidazole conjugate of Calix 4 arene and delineation of the features of the complex by molecular dynamics. ACS Appl Mater Int 5(24):13448–13456

[4] Salinas Y, Martinez-Manez R, Marcos MD, Sancenon F, Costero AM, Parra M, Gil S (2012) Optical chemosensors and reagents to detect explosives. Chem Soc Rev 41(3):1261–1296

[5] Bandela AK, Bandaru S, Rao CP (2015) A fluorescent 1,3-diaminonaphthalimide conjugate of Calix 4 arene for sensitive and selective detection of trinitrophenol: spectroscopy,

microscopy, and computational studies, and its applicability using cellulose strips. Chem-Eur J 21(38):13364–13374
[6] Toal SJ, Trogler WC (2006) Polymer sensors for nitroaromatic explosives detection. J Mater Chem 16(28):2871–2883
[7] Walsh ME (2001) Determination of nitroaromatic, nitramine, and nitrate ester explosives in soil by gas chromatography and an electron capture detector. Talanta 54(3):427–438
[8] Sylvia JM, Janni JA, Klein JD, Spencer KM (2000) Surface-enhanced Raman detection of 1,4-dinitrotoluene impurity vapor as a marker to locate landmines. Anal Chem 72(23):5834–5840
[9] Sun X, Wang Y, Lei Y (2015) Fluorescence based explosive detection: from mechanisms to sensory materials. Chem Soc Rev 44(22):8019–8061
[10] Li J, Kendig CE, Nesterov EE (2007) Chemosensory performance of molecularly imprinted fluorescent conjugated polymer materials. J Am Chem Soc 129(51):15911–15918
[11] Zhou L-L, Li M, Lu H-Y, Chen C-F (2016) Benzo 5 helicene-based conjugated polymers: synthesis, photophysical properties, and application for the detection of nitroaromatic explosives. Polym Chem 7(2):310–318
[12] Niu Q, Gao K, Wu W (2014) Cellulose nanofibril based graft conjugated polymer films act as a chemosensor for nitroaromatic. Carbohyd Polym 110:47–52
[13] Yang JS, Swager TM (1998) Fluorescent porous polymer films as TNT chemosensors: electronic and structural effects. J Am Chem Soc 120(46):11864–11873
[14] Leng H, Niu Q, Wu W (2013) Insoluble porous conjugated polymer films via phase separation and photo-crosslinking for the trace detection of 2,4-dinitrotoluene. Polym Int 62(8):1187–1191
[15] Isogai A, Saito T, Fukuzumi H (2011) TEMPO-oxidized cellulose nanofibers. Nanoscale 3(1):71–85
[16] Fukuzumi H, Saito T, Wata T, Kumamoto Y, Isogai A (2009) Transparent and high gas barrier films of cellulose nanofibers prepared by TEMPO-mediated oxidation. Biomacromol 10(1):162–165
[17] Saito T, Uematsu T, Kimura S, Enomae T, Isogai A (2011) Self-aligned integration of native cellulose nanofibrils towards producing diverse bulk materials. Soft Matter 7(19):8804–8809
[18] Zheng Q, Cai Z, Ma Z, Gong S (2015) Cellulose nanofibril/reduced graphene oxide/carbon nanotube hybrid aerogels for highly flexible and all-solid-state supercapacitors. Acs Appl Mater Int 7(5):3263–3271
[19] Feng J, Li Y, Yang M (2010) Conjugated polymer-grafted silica nanoparticles for the sensitive detection of TNT. Sens Actuator B Chem 145(1):438–443
[20] Wang X, Guo Y, Li D, Chen H, R-C Sun (2012) Fluorescent amphiphilic cellulose nanoaggregates for sensing trace explosives in aqueous solution. Chem Commun 48(45):5569–5570
[21] Ding L, Liu Y, Cao Y, Wang L, Xin Y, Fang Y (2012) A single fluorescent self-assembled monolayer film sensor with discriminatory power. J Mater Chem 22(23):11574–11582
[22] Huang F, Wu HB, Wang D, Yang W, Cao Y (2004) Novel electroluminescent conjugated polyelectrolytes based on polyfluorene. Chem Mater 16(4):708–716
[23] Gao K, Shao Z, Wang X, Zhang Y, Wang W, Wang F (2013) Cellulose nanofibers/multi-walled carbon nanotube nanohybrid aerogel for all-solid-state flexible supercapacitors. RSC Adv 3(35):15058–15064
[24] Leng H, Wu W (2012) Synthesis of a novel fluorene-based conjugated polymer with pendent bulky caged adamantane moieties and its application in the detection of trace DNT explosives. React Funct Polym 72(3):206–211
[25] Liu T, Ding L, Zhao K, Wang W, Fang Y (2012) Single-layer assembly of pyrene end-capped terthiophene and its sensing performances to nitroaromatic explosives. J Mater Chem 22(3):1069–1077
[26] Gao K, Shao Z, Li J, Wang X, Peng X, Wang W, Wang F (2013) Cellulose nanofiber-graphene all solid-state flexible supercapacitors. J Mater Chem A 1(1):63–67
[27] Cornil J, dos Santos DA, Crispin X, Silbey R, Brédas JL (1998) Influence of interchain interactions on the absorption and luminescence of conjugated oligomers and polymers: a quantum-chemical characterization. J Am Chem Soc 120(6):1289–1299
[28] Pella PA (1976) Generator for producing trace vapor concentrations of 2,4,6-trinitrotoluene, 2,4-dinitrotoluene, and ethylene glycol dinitrate for calibrating explosives vapor detectors. Anal Chem 48(11):1632–1637
[29] Zhu W, Tao S, C-A Tao, Li W, Lin C, Li M, Wen Y, Li G (2011) Hierarchically imprinted porous films for rapid and selective detection of explosives. Langmuir 27(13):8451–8457
[30] Wang D-H, Cui Y-Z, Tao F-R, Niu Q-F, Li T-D, Xu H (2016) A novel film of conjugated polymer grafted onto gelatin for detecting nitroaromatics vapor with excellent inhibiting photobleaching. Sens Actuator B Chem 225:319–326
[31] He G, Zhang G, Lue F, Fang Y (2009) Fluorescent film sensor for vapor-phase nitroaromatic explosives via monolayer assembly of oligo(diphenylsilane) on glass plate surfaces. Chem Mater 21(8):1494–1499
[32] Beyazkilic P, Yildirim A, Bayindir M (2014) Formation of pyrene excimers in mesoporous ormosil thin films for visual detection of nitro-explosives. ACS Appl Mater Int 6(7):4997–5004
[33] Salinas Y, Martinez-Manez R, Marcos MD, Sancenon F, Costero AM, Parra M, Gil S (2012) Optical chemosensors and reagents to detect explosives. Chem Soc Rev 41(3):1261–1296